



# Phase equilibria and Heusler phase stability in the Cu-rich portion of the Cu–Al–Mn system

R. Kainuma, N. Satoh<sup>1</sup>, X.J. Liu, I. Ohnuma, K. Ishida\*

*Department of Materials Science, Tohoku University, Sendai 980-77, Japan*

Received 11 July 1997

## Abstract

Results pertaining to the phase equilibria between the phases  $\alpha$  (A1),  $\beta$  (A2, B2 or  $L2_1(D0_3)$ ) and  $\gamma$  ( $\gamma$ -bronze type), and the two-stage order–disorder transition and decomposition reaction  $A2-B2-L2_1$  in the ternary system Cu–Al–Mn are reported. Ternary isothermal section diagrams at 800, 700, 600 and 550°C have been constructed using Energy Dispersion X-ray Spectrometry (EDX) analysis results, and it is found that the  $\beta$  single-phase region in the Cu–Al system is very significantly widened on increasing the Mn content. The critical temperatures ( $T_c$ ) of the  $A2-B2-L2_1$  order–disorder transitions, determined by Differential Scanning Calorimetry (DSC) analysis are found to be strongly dependent on the Al content rather than on the Mn content. It is confirmed by DSC measurements and TEM-EDX analysis that a miscibility gap island between  $Cu_3Al$  and  $Cu_2AlMn$  phases exists in the  $L2_1$  phase region. The second order ordering reaction between  $D0_3$  and  $L2_1$  structures has also been detected by X-ray diffraction. The stability of the bcc  $\beta$  phase is discussed in terms of atomic and magnetic ordering. © 1998 Elsevier Science S.A.

*Keywords:* Heusler alloy; Phase equilibria; Order–disorder transition; Miscibility gap island; Magnetic transformation

## 1. Introduction

Phase equilibria in the binary Cu–Al system have been studied extensively [1–3] as it is one of the basic systems constituting the ternary Cu-based shape memory alloys. In this system, the  $\beta$  phase with the bcc A2 structure undergoes a two-stage order–disorder transition: A2 (disordered bcc Cu)–B2 (CuAl)– $D0_3$ ( $Cu_3Al$ ) as shown in Fig. 1 [3]. The bcc  $\beta$  phase also exhibits a martensitic transformation. Several investigators have reported that the addition of Mn to the binary Cu–Al alloy stabilizes the bcc phase and widens the single phase region [4,5]. The composition region of the metastable ferromagnetic Heusler  $L2_1$  ( $Cu_2AlMn$ ) phase with unique magnetic properties [6–9] is located within the composition range of the  $\beta$  single phase. The corresponding stable phases in this composition region and in the low temperature range below 400°C are  $Cu_3Mn_2Al$ ,  $\gamma$  ( $\gamma$ -bronze type) and  $\beta$ -Mn ( $\beta$ -Mn type), but not the  $\beta$  phase [5,10–15]. Recently, the present authors have found that the ductility of the Heusler alloys with low Al contents is remarkably improved by decreasing the degree of long range order [16,17] and also

that the  $\beta$  phase with such a low degree of order or even with no order at all, exhibits a thermoelastic martensitic transformation with accompanying shape memory (SM) and pseudo-elasticity (PE) effects [16,17]. This finding has renewed the interest in this group of Cu-base alloys as new ductile SM materials.

Quite apart from the shape memory effect, the  $\beta$  alloys of the Cu–Al–Mn system also exhibit several other features which are interesting from the point of view of phase stability and magnetic properties: (1) A two-stage order–disorder transition  $A2-B2-L2_1$  occurs in the wide composition range of the  $\beta$  phase, and a miscibility gap along the  $Cu_3Al$ – $Cu_2AlMn$  pseudo-binary exists in the  $L2_1$  single phase region in the temperature range below 400°C [9,18–22]. (2) the ferromagnetism of the  $L2_1$  phase results from atomic ordering of the manganese atoms, and the magnetic properties such as the saturation magnetic moment depend on the degree of order of the Mn atoms [9]. Very recently, we have also found that the phase decomposition reaction  $D0_3+L2_1$  in the melt-spun ribbons gives rise to giant magnetoresistance (GMR) [23].

It is the purpose of this article to report mainly the results of investigations on the phase equilibria including the two-stage ordering reaction, the crystal structures and the Curie temperatures of the Cu-rich Cu–Al–Mn alloys in

\*Corresponding author.

<sup>1</sup>Kawasaki Steel Corporation, Chiba 260, Japan

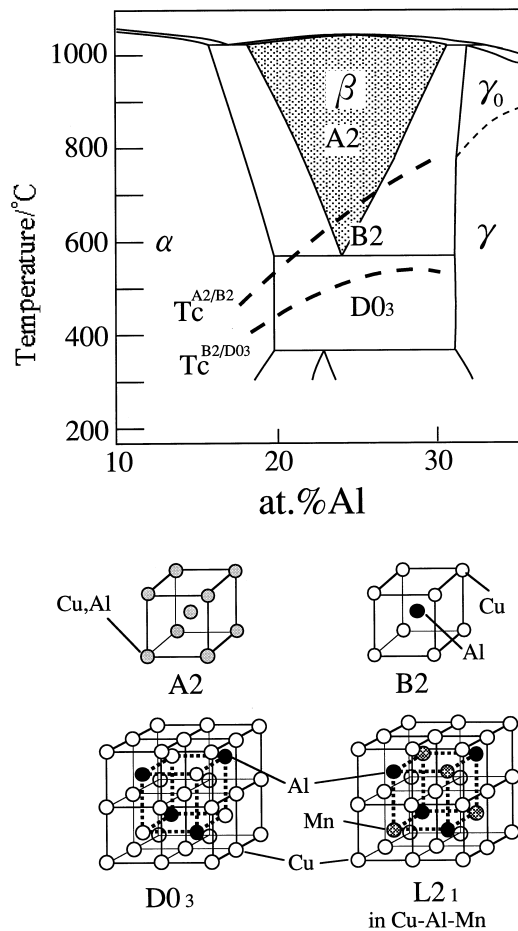


Fig. 1. Phase diagram of the Cu–Al system showing the A2–B2 and B2–D0<sub>3</sub> order–disorder transition temperatures [2].

a wide composition range and to clarify the characteristic features of the decomposition reaction in the  $\beta$  phase region of the Cu–Al–Mn system.

## 2. Experimental procedures

About 200 g quantities of each of alloys in the composition range of Cu–(0 to 40) at% Al–(0 to 30) at% Mn were prepared by induction melting of pure Cu(99.9%), Al(99.7%) and Mn(99.9%) in an argon atmosphere. The alloy ingots thus obtained were hot-rolled down at 800°C to sheets of thickness of about 2.5 mm, and then solution-treated at 900°C for 20 min. Some less workable ingots were directly annealed without hot-rolling.

The microstructures of specimens were examined by optical microscopy after a solution-treatment followed by equilibration at 550, 600, 700 and 800°C for 48 to 336 h. The equilibrium compositions of the  $\alpha$ ,  $\beta$  and  $\gamma$  phases after equilibration were determined by energy dispersion

X-ray spectroscopy (EDS) using a standard calibration method.

Powder specimens were analyzed by X-ray diffraction techniques using Cu-K $\alpha$  radiation to identify and characterize the phases present at room temperature and at 400°C. For determining the atomic configuration of the L<sub>21</sub> structure, the peak-intensities of  $\{111\}_{L2_1}$  and  $\{200\}_{L2_1}$  ordered reflections were obtained from each specimen by step-scanning for a 30-s step<sup>-1</sup> at  $2\theta=0.02^\circ$  steps. Transmission electron microscopy (TEM) examinations including EDS analysis were also carried out in a Hitachi H-800 analytical electron microscope on thin foils prepared by jet polishing in a solution consisting of 250 cm<sup>3</sup> phosphoric acid + 250 cm<sup>3</sup> ethanol + 50 cm<sup>3</sup> propanol + 500 cm<sup>3</sup> water + 5 g urea. Critical temperatures corresponding to the order–disorder transition and decomposition reactions were determined either by differential scanning calorimetry (DSC) or by differential thermal analysis (DTA). The heating and cooling rates employed for detecting the ordering and decomposition reactions were 10°C min<sup>-1</sup> and 2°C min<sup>-1</sup>, respectively. Magnetic transition temperatures were determined by the magnetic balance method (MB) at a heating rate of about 10°C min<sup>-1</sup>.

## 3. Results

### 3.1. Phase equilibria between the $\alpha$ , $\beta$ and $\gamma$ phases

Fig. 2(a) and Fig. 2(b) show the typical  $\alpha$  (A1) +  $\beta$  and  $\beta$  +  $\gamma$  two-phase microstructures taken from specimens of Cu-13 at% Al-15 at% Mn and Cu-37 at% Al-15 at% Mn alloys respectively equilibrated at 700°C for 48 h. The compositions of the  $\alpha$ ,  $\beta$  and  $\gamma$  phases at equilibrium, determined by EDS analysis are shown in Table 1 and Fig. 3. It is seen that the addition of Mn to Cu–Al alloys stabilizes the  $\beta$  phase and widens the  $\beta$  phase region. Vertical sections at fixed Mn composition of 10, 15 and 20 at% shown in Fig. 4 indicate that the  $\beta$  phase region extends to lower temperatures with increasing Mn content. The present results are in agreement with those reported by West and Thomas [5].

### 3.2. Order–disorder transition temperatures in the $\beta$ phase

Critical temperatures associated with the two-stage order–disorder transition, A2–B2–L<sub>21</sub>, are difficult to measure in the Cu–Al binary alloys because of the pronounced tendency of the  $\beta$  phase to decompose during heating in the DSC cell. However, in the case of Cu–Al–Mn alloys where this tendency is suppressed, they can be determined by DTA and DSC measurements. Fig. 5 shows a typical DTA cooling curve, where the critical tempera-

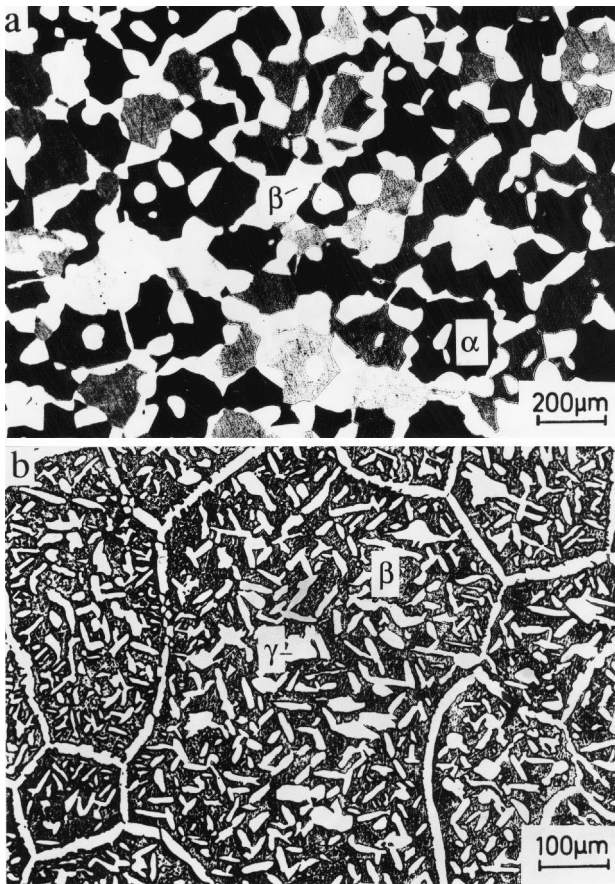


Fig. 2. Microstructure of (a) Cu-13 at% Al-15 at% Mn and (b) Cu-37 at% Al-15 at% Mn alloys quenched from 700°C.

tures,  $T_m$ ,  $T_c^{A2/B2}$  and  $T_c^{B2/L21}$  corresponding to solidification, A2–B2 and B2–L<sub>21</sub> ordering reactions respectively are marked. The critical temperatures so measured on different alloys are presented in Table 2, Fig. 4 and Fig. 6. It is seen that both the ordering temperatures corresponding to the A2–B2 and B2–L<sub>21</sub> reactions depend strongly on the Al content rather than on the Mn content. The DTA results from the present investigation are in agreement with the DTA results of Bouchard and Thomas [19]. It is worth noting that the critical temperatures corresponding to the two ordering stages in the Cu–Al binary system can be estimated by extrapolating from the ternary system data as shown in Fig. 7.

### 3.3. Decomposition in the ordered phase region

Fig. 8 shows the DSC heating curves obtained on several Cu<sub>3</sub>Al–Cu<sub>2</sub>AlMn pseudobinary alloys aged at 200°C. The temperature corresponding to the minimum point of the endothermic peak has been taken as the critical temperature. It is seen from the DSC traces associated with specimens containing more than 8 at.% Mn that the peaks begin to broaden with increasing Mn content, splitting into

Table 1

Phase equilibria between  $\alpha$  and  $\beta$  phases, and between  $\beta$  and  $\gamma$  phases

Temperature, °C	$\alpha$ , at%		$\beta$ , at%		$\gamma$ , at%	
	Mn	Al	Mn	Al	Mn	Al
800	4.9	14.7	5.4	18.5	–	–
	9.9	12.0	10.7	15.3	–	–
	14.6	10.5	15.6	13.1	–	–
	20.1	8.5	21.5	10.5	–	–
	26.0	7.8	26.9	10.0	–	–
	–	–	5.7	28.8	2.8	31.9
	–	–	10.1	30.1	4.1	32.5
	–	–	12.7	36.0	3.1	33.4
700	–	–	8.5	39.8	2.3	35.8
	5.1	15.4	5.5	19.1	–	–
	10.2	13.2	11.0	16.5	–	–
	15.0	11.7	16.3	15.2	–	–
	19.4	9.8	20.5	12.7	–	–
	24.7	10.0	25.3	12.6	–	–
	–	–	7.2	29.1	2.6	32.0
	–	–	16.9	33.7	2.9	32.3
600	–	–	21.5	40.7	1.9	32.8
	–	–	14.0	44.9	1.5	35.4
	5.1	16.2	5.7	20.1	–	–
	10.3	14.0	11.8	16.8	–	–
	14.4	12.3	16.0	15.6	–	–
	18.4	11.0	20.0	13.8	–	–
550	–	–	9.4	27.7	2.8	32.3
	–	–	11.3	25.9	2.8	32.2
	5.1	16.3	6.2	20.0	–	–
	10.3	14.5	12.2	17.0	–	–
	14.4	13.0	16.4	16.2	–	–
	18.4	11.3	20.0	14.7	–	–
–	–	11.0	24.7	2.7	29.8	
–	–	11.2	23.2	2.6	30.0	

two peaks, a sharp one and a broad one. The sharp peak is due to the magnetic transition ( $T_c^{mag}$ ) and the broad one to the redissolution of the D0<sub>3</sub> and L<sub>21</sub> phases ( $T_c^{seg}$ ). All the critical temperatures,  $T_c^{seg}$  and  $T_c^{mag}$  determined by DSC are listed in Table 2 and plotted in Fig. 9. It is seen that the temperature  $T_c^{seg}$  decreases sharply with decreasing Al content and the summit temperature for  $T_c^{seg}$  is located between 15–20 at% Mn. Fig. 10 shows the TEM bright field image (BFI) and the selected area diffraction pattern (SADP) taken from a Cu-25 at.% Al-15 at.% Mn specimen aged at 300°C for 83 h. It was confirmed that the SADP obtained from a region labeled A in the BFI was basically the same as that labeled B. This suggests that the two-phase structure consists of both the ordered bcc (D0<sub>3</sub> and L<sub>21</sub>) phases with the ordered reflections  $\{111\}_{D0_3}$  and  $\{200\}_{L21}$ . There are mis-fit dislocation networks in the phase boundaries and the phase labeled  $\beta$  has a tweed-like structure. TEM-EDS examination of the composition of A and  $\beta$  phases reveals that A and  $\beta$  correspond to Cu<sub>2</sub>AlMn and Cu<sub>3</sub>Al respectively as shown in Table 3 and Fig. 11. All these microstructural features are comparable to those

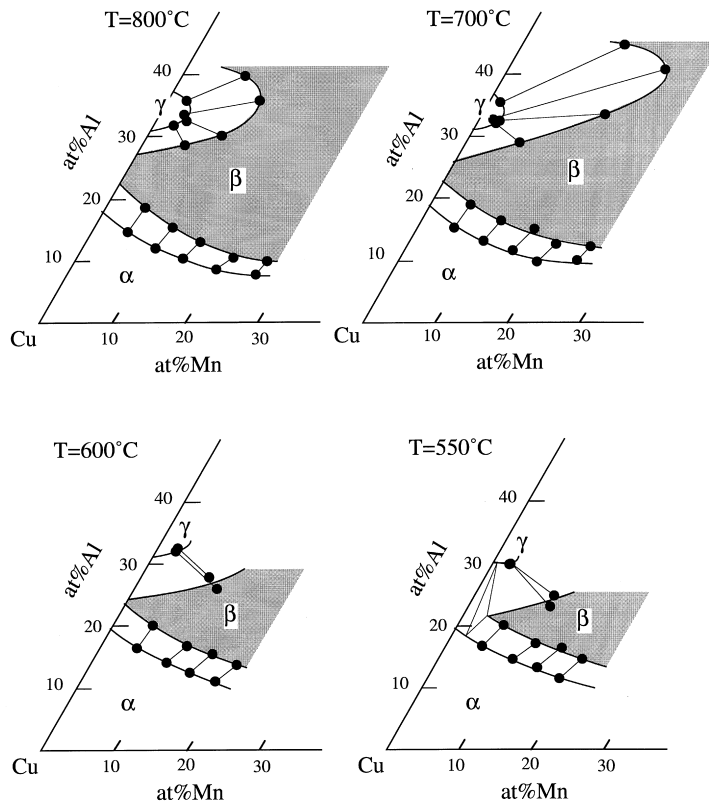


Fig. 3. Isothermal section diagrams for the Cu–Al–Mn ternary alloys.

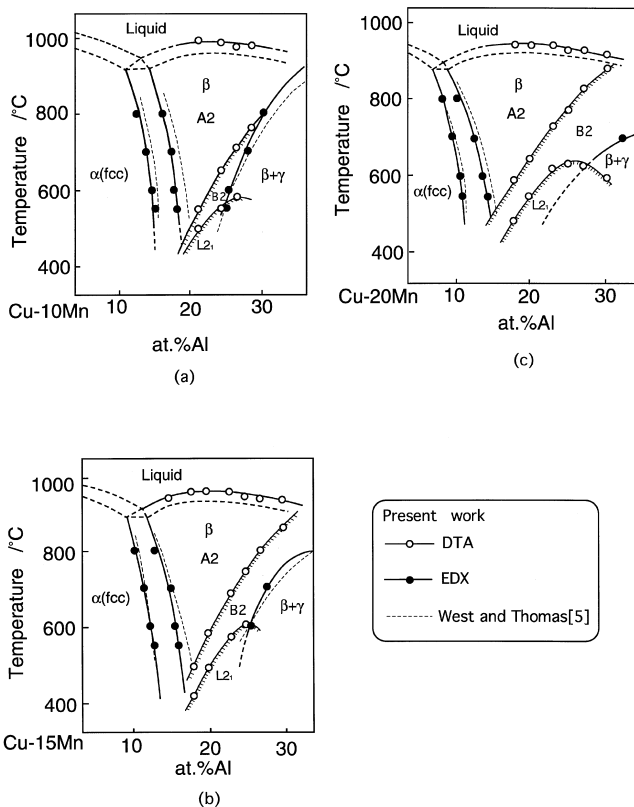


Fig. 4. Vertical section diagrams for Cu–Al–10 at% Mn, –15 at% Mn and –20 at% Mn alloys.

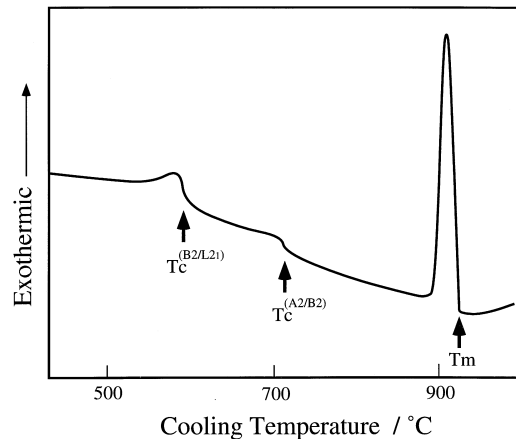


Fig. 5. DTA trace from a Cu-25 at% Al-15 at% Mn alloy specimen.

reported by Bouchard and coworkers [19,20]. The results of the TEM-EDS examination are in agreement with those of DSC measurement as shown in Fig. 11. It is also seen that a closed miscibility gap island is formed between  $\text{Cu}_3\text{Al}$  and  $\text{Cu}_2\text{AlMn}$  phases as shown in Fig. 11(b).

### 3.4. Configuration of manganese atoms in the ordered BCC phase

Fig. 12(a) and Fig. 12(b) show respectively the XRD pattern taken from the Cu-25 at% Al-25 at% Mn Heusler

Table 2  
Critical temperatures of order–disorder and magnetic transitions and segregation determined by thermal analysis

Specimen (at%)	$T_c^{A2/B2}$ (°C)	$T_c^{B2/L2_1}$ (°C)	$T_m$ (°C) (Liquidus)	$T_c^{mag}$ (°C)	$T_c^{seg}$ (°C)
Mn–Al					
5–25	679	541	–	–	248
6–25	–	–	–	–	272
7–25	–	–	–	–	285
8–25	–	–	–	–	299
9–25	–	–	–	300*	307
10–20	551	489	991	–	–
10–23	647	549	984	–	247
10–25	710	582	974	300* (~85)	313
10–27	781	–	980	–	–
15–18	493	437	951	–	–
15–20	582	498	951	–	218
15–23	685	571	949	–	293
15–25	742	604	934	298*	328
15–27	798	–	933	–	–
15–30	854	–	928	–	–
20–18	593	482	945	–	–
20–20	646	548	936	–	217
20–23	734	621	941	–	279
20–25	775	635	932	306*	328
20–27	830	630	932	–	–
20–30	886	–	922	–	–
22.5–25	–	–	–	302 (318)	–
24–25	–	–	–	329 (346)	271
25–20	648	587	931	(244)	–
25–23	–	–	–	(258)	–
25–25	794	644	933	(368)	–

( ) Magnetic balance.\* Two-phase specimen.

alloy and the lattice constant data obtained from the  $Cu_3Al$ – $Cu_2AlMn$  pseudobinary alloys aged at 500°C for 30 min after quenching from 800°C, along with the previous literature data [18,23]. It is seen that the lattice constant of the  $D0_3(L2_1)$  alloys increases linearly with increasing Mn content. All the specimens aged at temperatures between 350–550°C exhibit an XRD pattern similar

to Fig. 12(a), differing only in the relative intensity between some order peaks as shown in Fig. 13. There are only three types of Bragg reflections appearing in the X-ray diffraction patterns [8]:

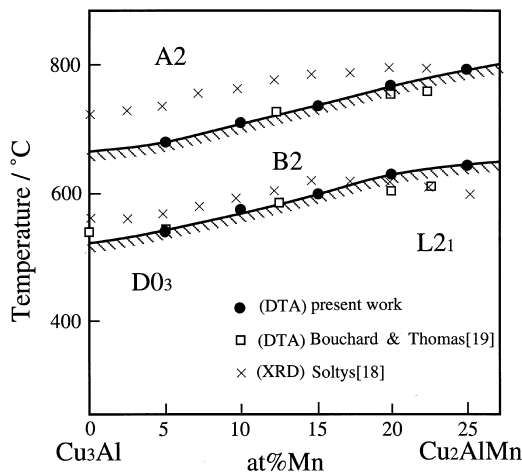


Fig. 6. Critical temperatures corresponding to the A2–B2 and B2– $D0_3(L2_1)$  order–disorder transition.

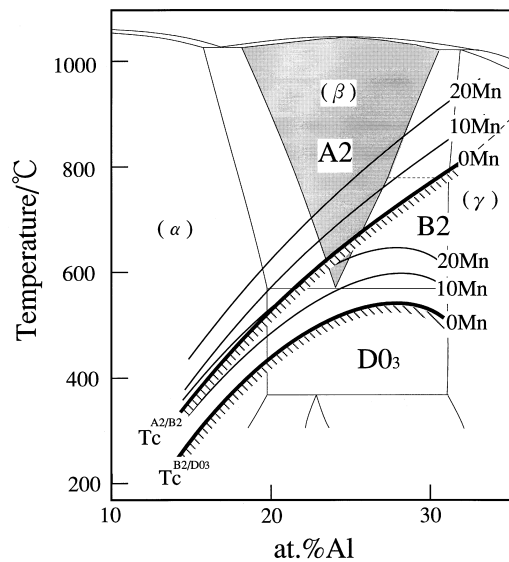


Fig. 7. Critical temperatures corresponding to the A2–B2 and B2– $D0_3$  order–disorder transition in Cu–Al binary alloys estimated by extrapolation from those corresponding to the Cu–Al–Mn alloys.

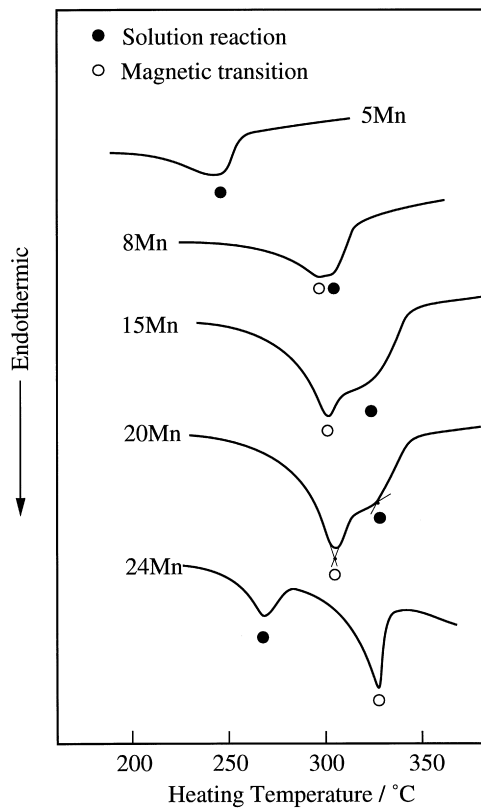


Fig. 8. DSC traces showing the dissolution reaction of the  $D0_3 + L2_1$  two-phase structure in the Cu-25 at% Al-Mn alloys.

$$h, k, l \text{ odd: } F_{hkl} = [(f_A - f_B)^2 + (f_C - f_D)^2]^{1/2}, \quad (1)$$

$$h, k, l \text{ even and } (h + k + l)/2 = 2n + 1: \\ F_{hkl} = f_A + f_B - f_C - f_D, \quad (2)$$

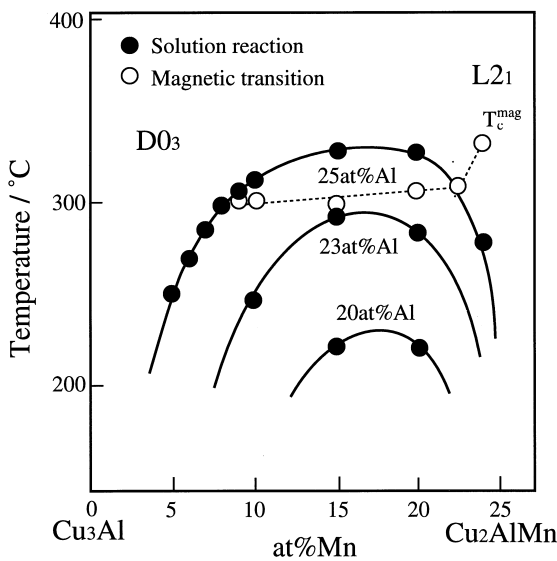


Fig. 9. Critical temperatures corresponding to the the  $D0_3 + L2_1$  two-phase boundaries and to magnetic transitions in the Cu-Al-Mn alloys determined by DSC measurements.

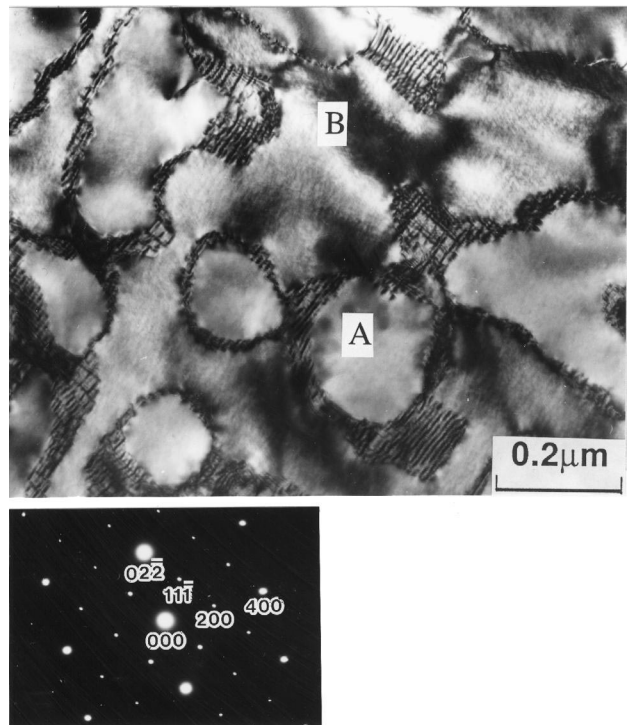


Fig. 10. TEM micrograph showing the  $D0_3(B:Cu_3Al) + L2_1(A:Cu_2AlMn)$  two-phase structure in the Cu-25 at% Al-15 at% Mn specimen reannealed at 300°C for 83 h after annealing at 800°C for 1 h.

$$h, k, l \text{ even and } (h + k + l)/2 = 2n: \\ F_{hkl} = f_A + f_B + f_C + f_D, \quad (3)$$

where  $f_A$ ,  $f_B$ ,  $f_C$  and  $f_D$  denote the atomic scattering amplitudes of atoms occupying the sublattice A, B, C and D. The intensities of all reflections depend on the alloy composition, and only the reflections of the type (1) and (2) are functions of the degree of atomic order. Therefore, it would be interesting to know what the effect of Mn content would be on the relative intensity ratio  $I_{(111)}/I_{(200)}$  between the  $\{111\}$  and  $\{200\}$  peaks which would be a measure of the type of order of Mn atoms. Fig. 14(a) shows the experimentally obtained relative intensity ratios  $I_{(111)}/I_{(200)}$  in the  $Cu_3Al-Cu_2AlMn$  pseudobinary alloys

Table 3  
Phase equilibria between  $Cu_3Al$  and  $Cu_2AlMn$  phases

Temperature, °C	$Cu_3Al$ , at%		$Cu_2AlMn$ , at%	
	Mn	Al	Mn	Al
300	8.3	24.0	23.4	26.1
	5.5	26.9	22.6	27.4
280	7.6	24.6	24.2	25.5
	10.4	22.6	22.8	23.4
260	5.6	23.5	22.7	26.0
	6.9	22.7	24.3	23.0
	4.8	27.0	21.6	27.4

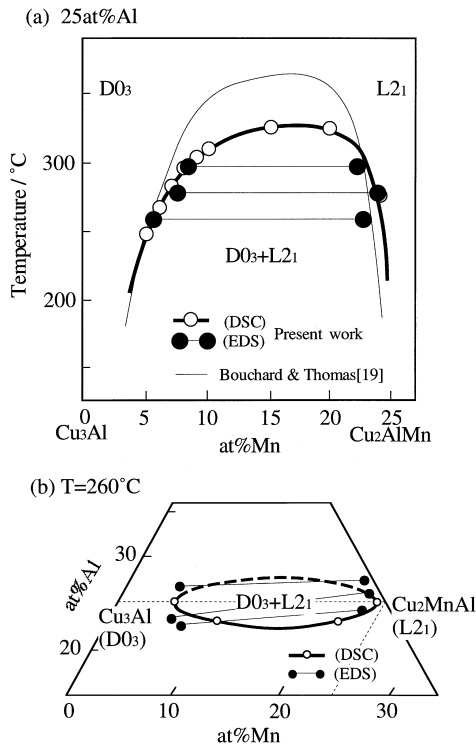


Fig. 11. Phase equilibrium between the DO<sub>3</sub> and L<sub>21</sub> phases determined by TEM-EDS and DSC measurements.

along with calculated ones. The calculations have been carried out assuming that the atomic configurations are such that  $f_A = f_B = f_{Cu}$ ,  $f_C = f_{Cu+Mn}$  (: mixture of  $f_{Cu}$  and  $f_{Mn}$ ) and  $f_D = f_{Al}$  for the L<sub>21</sub> structure, and  $f_A = f_B = f_C = f_{Cu+Mn}$  and  $f_D = f_{Al}$  for the DO<sub>3</sub> structure. The relative intensity ratio  $I_{(111)}/I_{(200)}$  is about 2.0 in alloys with up to 8 at% Mn and this corresponds to the ideal DO<sub>3</sub> structure. It changes drastically in a composition region between 8 and 9 at% Mn and decreases continuously with increasing Mn content to the value corresponding to the ideal L<sub>21</sub> structure. The results of the in-situ examinations at 400°C are also in agreement with that obtained from the quenched specimens as plotted in Fig. 14(a). This drastic change in the  $I_{(111)}/I_{(200)}$  ratio at about 8 at% Mn is to be attributed to the change in the type of order of Mn atoms brought about by a change from the DO<sub>3</sub> to the L<sub>21</sub> structure. The compositions corresponding to this sharp change in as-quenched specimens are plotted in Fig. 14(b), from which it can be seen that an ordering transition DO<sub>3</sub>-L<sub>21</sub> involving Mn atoms occurs between 7 and 10 at% Mn. However, there is neither experimental nor theoretical evidence to suggest that a DO<sub>3</sub>/L<sub>21</sub> ordering transition exists in any other systems.

### 3.5. Ferromagnetic transition

The Curie temperatures of Heusler alloys have been determined by a combination of magnetic balance (MB) and DSC methods as shown in Fig. 15. The complicated nature of the magnetization vs. temperature curve in the

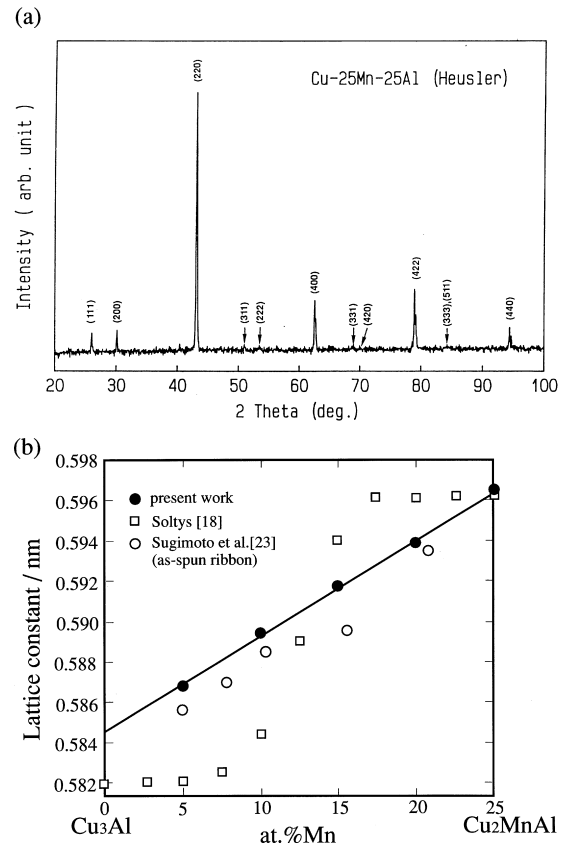


Fig. 12. (a) XRD pattern obtained from the Cu<sub>2</sub>AlMn alloy aged at 500°C for 30 min after annealing at 800°C for 1 h, and (b) lattice constants of the Cu-25 at% Al-Mn alloys determined by XRD.

case of the Cu-25 at% Al-10 at% Mn alloy shown is explained as follows: The peak at about 230°C in the magnetisation curve is the result of spinodal decomposition of the alloy in the DO<sub>3</sub>+L<sub>21</sub> miscibility gap. The Curie temperature in the case of this single phase alloy can however be estimated by extrapolating from the curve in the temperature region below 100°C. The Curie temperatures obtained by the MB measurement method are shown in Fig. 16 and Table 2, and they are about 16°C higher than those determined by using DSC. This difference in the  $T_c$ -mag values may be attributed to the way in which the Curie temperature has been defined in the DSC method.  $T_c$ -mag decreases with Mn content at the rate of 20°C/%Mn. It is interesting to note that the Curie temperature of the Cu-23 at% Al-25 at% Mn alloy is about 100°C lower than that of the Cu-25 at% Al-25 at% Mn stoichiometric Heusler alloy as plotted in Fig. 16(b).

## 4. Discussion

### 4.1. Formation of miscibility gap

In the present study, the phase equilibrium between the DO<sub>3</sub> and L<sub>21</sub> phases as shown in Fig. 11 has been

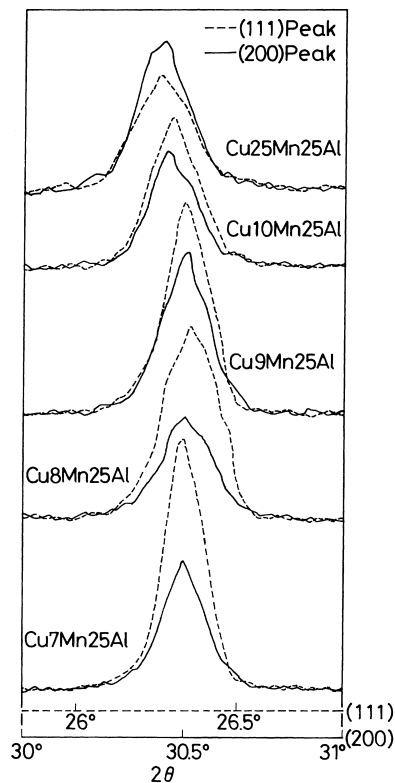


Fig. 13. (111) and (200) peaks from the XRD pattern obtained for the Cu-25 at% Al–Mn alloys aged at 400°C for 30 min.

determined only for alloys with Al contents below 25 at%. It would be very difficult to experimentally determine the phase equilibrium in alloys with higher Al contents, because the kinetics of the precipitation of the stable  $\gamma$  phase are so fast that only rapid solidification can suppress the formation of the  $\gamma$  phase. Very recently, we have reported the occurrence of GMR properties in the melt-spun ribbons of the Cu–Al–Mn alloys containing Al content from 20 to 30 at% and clarified that the region of GMR in the phase diagram has an elliptical shape corresponding to the two-phase region of the  $D0_3$  and  $L2_1$  phases [23]. This fact suggests that in the alloys with more than 25 at% Al also, the two-phase region may form a miscibility gap island with an elliptical shape as illustrated in Fig. 11.

An explanation for the formation of the miscibility gap in the  $\text{Cu}_3\text{Al}$ – $\text{Cu}_2\text{AlMn}$  pseudobinary system can be attempted on the basis of chemical ordering [24], magnetic ordering [25,26] and/or lattice mismatch effects related to differences in the lattice parameters between the two intermetallic phases [27].

#### 4.1.1. $D0_3/L2_1$ chemical ordering

The miscibility gap near the 5–10 at% Mn region has been carefully investigated to explore the possibility that a Nishizawa horn along the  $D0_3/L2_1$  ordering transition [25] may be present. The experimental results plotted in Fig. 9 confirm the absence of this type of miscibility gap in this

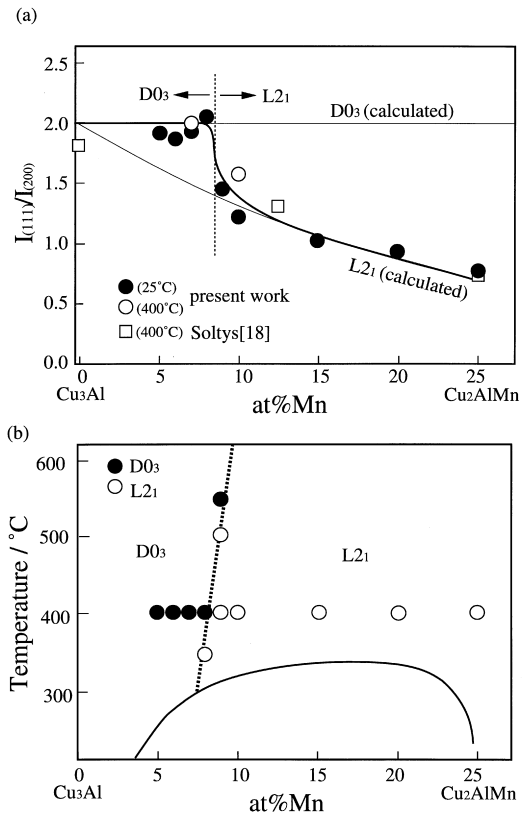


Fig. 14. (a) Relative intensity  $I_{(111)}/I_{(200)}$  ratios of the (111) and (200) peaks in the XRD pattern of the Cu-25 at% Al–Mn alloys. Solid lines indicate the calculated results assuming that the alloys possessed the  $D0_3((\text{Cu},\text{Mn})_3\text{Al})$  and  $L2_1(\text{Cu}_2(\text{Mn},\text{Cu})\text{Al})$  structures, respectively. (b) Critical boundary between the  $D0_3$  and  $L2_1$  structures determined by recourse to differences in relative intensity ratio.

system. It is known that even in the stoichiometric Heusler alloy the degree of order of Mn atoms strongly depends on the quenching temperature [9]. This fact suggests that the free-energy change and the driving force due to this

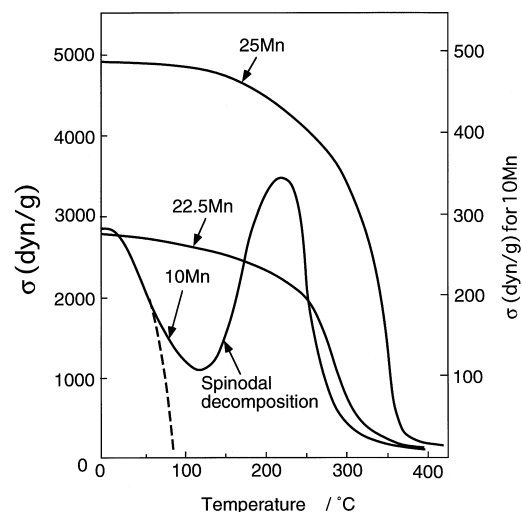


Fig. 15. Thermomagnetization traces showing the magnetic transition in the Cu-25 at% Al–Mn alloys.

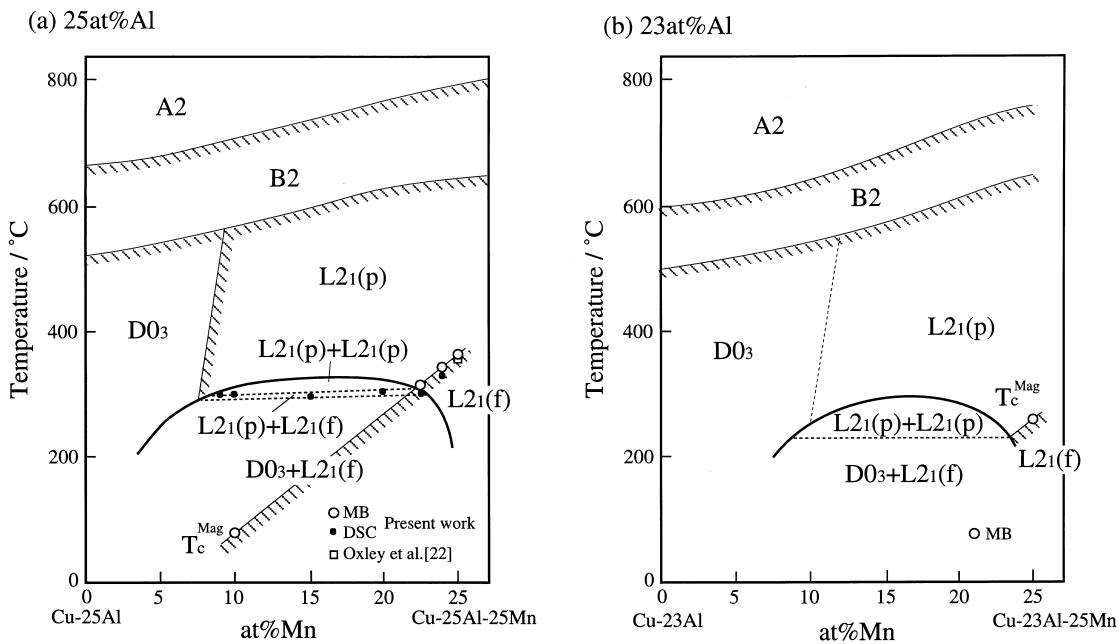


Fig. 16. Critical temperatures corresponding to the chemical ordering transitions, magnetic transitions, and phase decomposition in the Cu-25 at% Al–Mn and Cu-23 at% Al–Mn pseudobinary systems.

chemical ordering transition may not be sufficient enough to give rise to such a large miscibility gap.

#### 4.1.2. Magnetic ordering

The miscibility gap shown in Fig. 16 has an asymmetric shape with the summit point located at about 15 at% Mn. This points to the possibility that the magnetic contribution may not be inconsiderable in influencing this phase separation. However, it can be seen from Fig. 16, that the paramagnetic  $L_{21}(p)+L_{21}(p)$  two-phase region is formed below the summit temperature for both the Cu-25 at% Al–Mn and Cu-23 at% Al–Mn systems. The occurrence of such a two-phase region cannot be due to either chemical or magnetic ordering.

#### 4.1.3. Lattice mismatch effect

Recently, the present authors have reported that there exists a large difference in the lattice parameters between the B2 and  $L_{21}$  intermetallic compounds in the NiAl(B2)– $Ni_2AlTi(L_{21})$  and FeAl(B2)– $Fe_2AlTi(L_{21})$  pseudobinary systems and this is the predominant reason for the presence of the B2 +  $L_{21}$  miscibility gap [28]. The difference in the lattice parameter between the  $Cu_3Al$  and  $Cu_2AlMn$  alloys is about 2.0% as shown in Fig. 12(b), which is comparable to that in the NiAl– $Ni_2AlTi$  pseudobinary system. This fact suggests that this lattice mismatch effect can be one of the reasons for the formation of this miscibility gap. Further thermodynamic analysis will be needed to quantify the free energy differences between the constituent phases and clarify the origin and characteristic features of this miscibility gap.

## 5. Conclusions

1. The phase relationships between the  $\alpha$ ,  $\beta$  and the  $\gamma$  phases in the Cu-rich portion of the Cu–Al–Mn system have been established in the temperature interval between 550 and 800°C.
2. The critical order–disorder transformation temperatures for the reactions A2–B2 and B2– $L_{21}(D_{03})$  in the  $\beta$  phase have been determined. Both the ordering temperatures A2–B2 and B2– $L_{21}(D_{03})$  are strongly influenced by the Al content rather than by the Mn content.
3. A sharp change in the degree of order arising from the  $D_{03}$ – $L_{21}$  ordering of Mn is observed in the vicinity of 8–9 at% Mn content in the  $Cu_3Al$ – $Cu_2AlMn$  pseudobinary system.
4. The existence of a closed elliptical  $D_{03}+L_{21}$  miscibility gap with its summit temperature located at 320°C has been confirmed in the  $Cu_3Al$ – $Cu_2AlMn$  pseudobinary system.
5. The critical temperatures of magnetic ordering in the  $L_{21}$  alloys has also been determined for alloys in the Heusler phase region. The Curie temperature decreases with decreasing Mn and Al contents in these alloys.

## Acknowledgements

The authors wish to thank Dr.L.Chandrasekaran of DERA, UK for help in preparation of this manuscript for presentation. This work was supported by the Grant-in-aids for Scientific Research from the Ministry of Education,

Science, Sports and Culture, Japan. The authors also wish to thank the support from International Copper Association. One of the authors (R.K) would like to thank the support from The Mazda Foundation's Research Grant.

## References

- [1] J. Murray, in: P.R. Subramanian, D.J. Chakrabarti, D.E. Laughlin (Eds.), Phase Diagram of Binary Copper Alloys, ASM International, 1990, p. 18.
- [2] X.J. Liu, I. Ohnuma, R. Kainuma, K. Ishida, J. Alloys Comp., (1997) in press.
- [3] R. Hultgren, P.D. Desai, Selected Thermodynamic Values and Phase Diagrams for Copper and Some of its Binary Alloys, INCRA Monograph I Metallurgy of Copper, The International Copper Research Association (1971), 39.
- [4] J.P. Haworth, W. Hume-Rothery, Phil. Mag. 43 (1952) 613.
- [5] D.R.F. West, D.L. Thomas, J. Inst. Metals 85 (1956) 97.
- [6] F. Heusler, Verh. DPG5 (1903) 219 Z. Angew. Chem. 17 (1904) 260.
- [7] O. Heusler, Ann. Physik. 19 (1934) 155.
- [8] A.J. Bradley, J.W. Rodgers, Proc. Roy. Soc. London 144A (1934) 340.
- [9] G.B. Johnston, E.O. Hall, J. Phys. Chem. Solids 29 (1968) 193.
- [10] W. Koester, T. Godecke, Z. Metallkde 57 (1966) 889.
- [11] T. Yamane, H. Okamoto, J. Takahashi, Z. Metallkde 71 (1980) 813.
- [12] R. Kozubski, J. Soltys, J. Mater. Sci. 17 (1982) 1441.
- [13] R. Kozubski, J. Soltys, J. Mater. Sci. 18 (1983) 1689.
- [14] R. Kozubski, J. Soltys, R. Kuziak, J. Mater. Sci. 18 (1983) 3079.
- [15] R. Kozubski, J. Soltys, J. Dutkiewicz, J. Morgiel, J. Mater. Sci. 22 (1987) 3843.
- [16] R. Kainuma, S. Takahashi, K. Ishida, Metal. Mater. Trans. A 23A (1996) 2187.
- [17] R. Kainuma, S. Takahashi, K. Ishida, J. de Phys. IV, Colloque C8, 5 (1995) C8–961.
- [18] J. Soltys, Phys. Stat. Sol. (a) 63 (1981) 401.
- [19] M. Bouchard, G. Thomas, Acta Metall. 23 (1973) 1485.
- [20] M. Bouchard, R.J. Rivak, G. Thomas, Surface Sci. 31 (1972) 275.
- [21] M. Prado, M. Sada, F. Lovey, Scripta Metall. Mater. 28 (1993) 545.
- [22] D.P. Oxley, R.S. Tebble, K.C. Williams, J. Appl. Phys. 34 (1963) 1362.
- [23] S. Sugimoto, S. Kondo, H. Nakamura, et al. J. Alloys Comp., (1997) in press.
- [24] G. Inden, Acta Metall. 22 (1974) 945.
- [25] T. Nishizawa, J. Phase Equilibria 16 (1995) 379.
- [26] T. Takayama, S. Shinohara, K. Ishida, T. Nishizawa, J. Phase Equilibria 16 (1995) 390.
- [27] W.B. Pearson, W. Hume-Rothery, J. Inst. Metals, 80 (1951–52) 641.
- [28] R. Kainuma, K. Urushiyama, C.C. Jia, I. Ohnuma, K. Ishida, Mater. Sci. Eng., (1997) in press.